Acta Oceanol. Sin., 2021, Vol. 40, No. 10, P. 84–96
https://doi.org/10.1007/s13131-021-1828-9
http://www.aosocean.com
E-mail: ocean2@hyxb.org.cn

Optical properties and surface energy flux of spring fast ice in the Arctic

Jialiang Zhu[1], Yilin Liu[1], Xiaoyu Wang[2], Tao Li[1]*

[1] College of Oceanic and Atmospheric Sciences, Ocean University of China, Qingdao 266100, China

[2] Key Laboratory of Physical Oceanography, Ministry of Education, Qingdao 266100, China

Received 9 December 2020; accepted 19 February 2021

Abstract

Over the past decades, sea ice in the polar regions has been significantly affecting local and even hemispheric climate through a positive ice albedo feedback mechanism. The role of fast ice, as opposed to drift ice, has not been well-studied due to its relatively small coverage over the earth. In this paper, the optical properties and surface energy balance of land fast ice in spring are studied using *in situ* observations in Barrow, Alaska. The results show that the albedo of the fast ice varied between 0.57 and 0.85 while the transmittance increased from 1.3×10^{-3} to 4.1×10^{-3} during the observation period. Snowfall and air temperature affected the albedo and absorbance of sea ice, but the transmittance had no obvious relationship with precipitation or snow cover. Net solar shortwave radiation contributes to the surface energy balance with a positive 99.2% of the incident flux, with sensible heat flux for the remaining 0.8%. Meanwhile, the ice surface loses energy through the net longwave radiation by 18.7% of the total emission, while the latent heat flux accounts for only 0.1%. Heat conduction is also an important factor in the overall energy budget of sea ice, contributing 81.2% of the energy loss. Results of the radiative transfer model reveal that the spectral transmittance of the fast ice is determined by the thickness of snow and sea ice as well as the amount of inclusions. As major inclusions, the ice biota and particulates have a significant influence on the magnitude and distribution of the spectral transmittance. Based on the radiative transfer model, concentrations of chlorophyll and particulate in the fast ice are estimated at 5.51 mg/m^2 and 95.79 g/m^2, which are typical values in the spring in Barrow.

Key words: Arctic Ocean, fast ice, optical properties, energy flux, chlorophyll

Citation: Zhu Jialiang, Liu Yilin, Wang Xiaoyu, Li Tao. 2021. Optical properties and surface energy flux of spring fast ice in the Arctic. Acta Oceanologica Sinica, 40(10): 84–96, doi: 10.1007/s13131-021-1828-9

1 Introduction

Sea ice plays a key role in Arctic climate change because it controls the energy balance of the Arctic Ocean and affects global radiative forcing (Hudson, 2011). Recent studies have shown a decline in Arctic sea ice, including a reduction in the extent of summer sea ice (Comiso et al., 2008; Serreze et al., 2007; Stroeve et al., 2007), a decrease in sea ice thickness (Rothrock et al., 2008; Haas et al., 2008; Kwok and Rothrock, 2009), and an extension of the melt season (Markus et al., 2009). In addition, it has been confirmed that a majority of the ice cover has changed from multi-year ice to seasonal ice (Rigor and Wallace, 2004; Nghiem et al., 2007; Maslanik et al., 2007, 2011; Comiso, 2012). This shift has an impact on the morphologic, thermodynamic, and dynamic properties of the sea ice, which in turn affects its heat budget and mass balance (Perovich and Polashenski, 2012; Stroeve and Notz, 2018).

The apparent optical properties of sea ice, including its albedo, transmittance, and absorbance, determine the distribution of solar radiation reaching the ice surface, which affects the energy balance of sea ice. Those properties vary significantly with space and time (Grenfell and Perovich, 1984; Perovich, 1991; Perovich et al., 1998). The amount of attenuation is independent of the intensity or spectral distribution of the incident radiation (Qu et al., 2009). The albedo of different surface types of sea ice as well as its seasonal evolution have been quantitatively analyzed (Perovich et al., 1998; Gerland et al., 1999, 2004; Nicolaus et al., 2010; Perovich and Polashenski, 2012; Perovich and Richter-Menge, 2015). Inherent optical properties such as scattering and attenuation coefficients for the different types of sea ice have also been studied by Perovich (1990), Grenfell and Warren (1999), Light et al. (2008, 2015), and Malinka et al. (2016). However, continuing observations and analyses on the optical properties of sea ice are still essential due to the rapid changes in the Arctic sea ice in recent years.

Fast ice is one of the major parts of sea ice in the Arctic, especially around the ocean coast. Due to the similarity of optical properties in floe ice and land-fast ice (Grenfell and Perovich, 2004; Grenfell et al., 2006), observations on the easily accessible fast ice have become an important data source for the study of long-term changes in the sea ice. Previous studies have shown that the spatial variation of fast ice transmittance is mainly dependent on snow thickness. The peak of spectral transmittance ranges from 460 nm for pure ice to 500–550 nm for particulate ice (Perovich et al., 1998). Grenfell and Perovich compared the res-

Foundation item: The National Major Research High Resolution Sea Ice Model Development Program of China under contract No. 2018YFA0605903; the National Natural Science Foundation of China under contract No. 41776192; the Fundamental Research Funds for the Central Universities under contract No. 202165005.

*Corresponding author, E-mail: litaoocean@ouc.edu.cn

ults in Barrow between 2000 and 2002 with those in the central Arctic and found that the albedo of land-fast ice evolved one to two times faster than that of floes in the central Arctic (Grenfell and Perovich, 2004; Grenfell et al., 2007). Hamre et al. (2004) found that a 2.5-cm-thick layer of snow is less transparent than a 61-cm-thick layer of ice. Observations by Gradinger et al. in 2002 and 2003 revealed that the light transmitted through particulate-laden ice was reduced by more than 99% compared to pure sea ice (Gradinger et al., 2009). Nicolaus et al. (2010, 2013) found that the spatial variation of the transmittance is determined by both the thickness and the optical properties of the snow cover, and that it varies between one-third and three times its average value. However, the transmittance increased by 20 times from May to June, which means its seasonal variation far exceeds its spatial variation.

In addition to the surface characteristics of sea ice, inclusions in the ice interior such as particle matter and biomass significantly affect the optical properties of sea ice (Light et al., 1998; Grenfell et al., 2006; Nicolaus et al., 2013). Several previous studies at the Resolute Bay, Northwest Territories, Canada, have focused on the relationships among light transmission, snow cover, and biomass accumulation (Mundy et al., 2007; Campbell et al., 2014; Leu et al., 2015). These studies have analyzed a seasonal cycle of biological activities where increasing short wave radiation results in an initiation of algal growth in March or early April. Biological activities inside the continental ice are also one of the most significant factors affecting the radiation reaching the bottom of sea ice (Ehn et al., 2008a). Research by Xu et al. (2012) showed that the concentrations of particulate matter and colored dissolved organic matter in sea ice will move the peak of spectral albedo to a longer wavelength, and determined the absorbance at shortwave. Nicolaus et al. (2013) found that the amount of chlorophyll estimated from the observed transmittance is an order of magnitude larger than the observed value. A possible explanation observation is that the relatively high particulate matter in the fast ice affects the spectral transmittance.

In the studies mentioned above, observations and analysis were focused mainly on melting fast ice in summer, which has different physical and optical properties than the ice in spring. Moreover, because of global warming and Arctic amplification, the physical structure of sea ice has experienced some significant changes over the past decade (Barber et al., 2009, 2012), which is affecting the radiative transfer in the ice. Knowledge of the evolution of surface energy flux and optical properties of the fast ice is still largely lacking.

This paper is focused on the apparent optical properties and surface energy balance of the land-fast ice in spring. Information on the *in situ* observation and data processing method is introduced in Section 2. Section 3 contains a discussion of the distribution of radiative energy in the air-ice-ocean system, turbulent heat flux at the ice surface, heat conduction in the ice, and the use of a modified one-dimensional radiative transfer model to study the effect of included contents on sea ice optical properties and simulate the spectral albedo and transmittance of the fast ice. Finally, Section 4 contains a summary of the conclusions with some perspectives.

2 Data and methods

2.1 *In situ observations*

The measurements of apparent optical properties and energy balance were carried out in Barrow (71.336°N, 156.687°W), Alaska, from May 1 to 18, 2014 (Fig. 1). Integral and spectral albedo of the fast ice were measured using a CNR4 radiometer produced by KIPP&ZONEN and a Ramses ACC-VIS hyperspectral radiometer from TriOS (Figs 2a and b). The CNR4 has a wavelength coverage of 300–2 800 nm, recording four integral radiation components of downwelling shortwave, upwelling shortwave, downwelling longwave, and upwelling longwave (hereinafter called R_{sd}, R_{su}, R_{ld}, and R_{lu}, respectively). Spectral radiation was measured using a Ramses ACC-VIS, which has a wavelength coverage of 320–950 nm with an average spectral resolution of 3.3 nm. The Ramses ACC-VIS can observe the optical signals of 256 channels, of which about 190 bands are corrected and another 19 bands are used for correction. Observations of sea ice transmittance were made using a multi-spectral high-resolution profile reflection radiometer (PRR, Fig. 2c) produced by Biospherical Instruments (BSI), which includes two components: underwater instrument PRR800 and surface instrument PRR810. The spectral range of PRR800/810 is 305–875 nm with a total of 18 valid bands.

Two Ramses ACC-VIS spectroradiometers placed upward and downward were used to measure the downwelling and upwelling radiation (Fig. 3). Simultaneous measurement of incid-

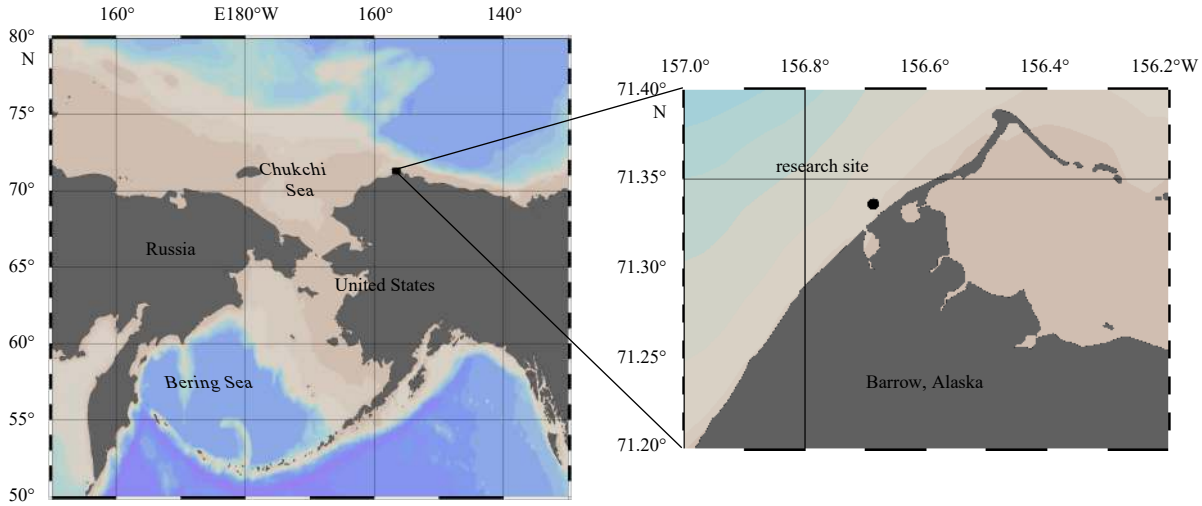

Fig. 1. Study site at Barrow, Alaska.

Fig. 2. Radiometers used in the observation. a. CNR4, b. Ramses ACC-VIS, and c. PRR800/810.

ent and reflected radiation is required when measuring the albedo of sea ice. The procedure for observing transmitted radiation is more complicated. First, an ice hole was drilled by ice auger, and the PRR800 spectroradiometer was lowered into the water. Next, the forepart of the holder arm was rotated 90° to ensure that the instrument was fixed on the bottom of the ice (Zhao and Li, 2010). After that, the PRR810 spectroradiometer was set above the surface to measure the incident radiation as a reference (Fig. 3). When the whole installation was set up, the ice hole was covered with snow to minimize damage to the surrounding field. Since changes in weather conditions will affect the light field, an automatic meteorological station was placed at a distance from the site of optical observation to collect the necessary variables including temperature, humidity, pressure, and wind speed (Fig. 3). Instruments on the site were maintained every day to avoid contamination from snow or water vapor. The temperature and salinity of the ice core were measured every 20 cm during each sampling period. In addition, data on cloud cover as well as weather and sky conditions were collected from websites (www.worldweatheronline.com and www.timeanddate.com).

2.2 *Calculation of the optical parameters*

Albedo, transmittance, and absorbance are crucial for evaluating the capability of fast ice to absorb solar radiation. The spectral albedo of sea ice is defined as

$$\alpha(\lambda) = \frac{F_{\mathrm{u}}(0,\lambda)}{F_{\mathrm{d}}(0,\lambda)}, \tag{1}$$

where $F_{\mathrm{u}}(0,\lambda)$ is the plane upward irradiance or reflected irradiance, and $F_{\mathrm{d}}(0,\lambda)$ is the plane downward irradiance or incident irradiance (0 represents the sea ice surface). The spectral characteristics of sea ice albedo depend mainly on the solar radiation absorption properties of the sea ice surface. Since the land-fast ice is a complex mixture of pure ice, air bubbles, brine bubbles, salt crystals, and terrestrial materials, the absorption of solar radiation by these components reveals different characteristics of albedo in different bands.

In polar climatology, the researchers focus on broadband albedo, or integral albedo, defined as

$$\alpha_{\mathrm{t}} = \frac{\int \alpha(\lambda) F_{\mathrm{d}}(0,\lambda)\mathrm{d}\lambda}{\int F_{\mathrm{d}}(0,\lambda)\mathrm{d}\lambda}. \tag{2}$$

The integral albedo depends not only on the spectral albedo of different bands but also on the spectral distribution of the incident radiation. As a result, changes in sky conditions, such as clouds, can lead to differences in integral albedo. In general, the integral albedo under cloudy skies is greater than the albedo under clear skies. The former is usually 8%–12% higher than the latter (Perovich and Gow, 1996).

The spectral transmittance of sea ice is defined as

$$T(z,\lambda) = \frac{F_{\mathrm{d}}(z,\lambda)}{F_{\mathrm{d}}(0,\lambda)}, \tag{3}$$

where $F_{\mathrm{d}}(z,\lambda)$ is the downward irradiance of the plane at a depth of z, and the corresponding integral transmittance is

$$T_{\mathrm{t}}(z) = \frac{\int \delta(\lambda) T(z,\lambda) F_{\mathrm{d}}(0,\lambda)\mathrm{d}\lambda}{\int \delta(\lambda) F_{\mathrm{d}}(0,\lambda)\mathrm{d}\lambda}. \tag{4}$$

The transmitted radiation $F_{\mathrm{d}}(z,\lambda)$ through the sea ice refers to the downward irradiance observed by the instrument at the bottom of the ice, in which case the subscript z can be omitted. The expression $\delta(\lambda)$ is the correction coefficient for atmospheric absorption, which is adopted by multispectral instruments. At wavelengths within the atmospheric absorption band, radiation needs to be corrected by $\delta(\lambda)$ ($\leqslant 1$). The correction coefficients of

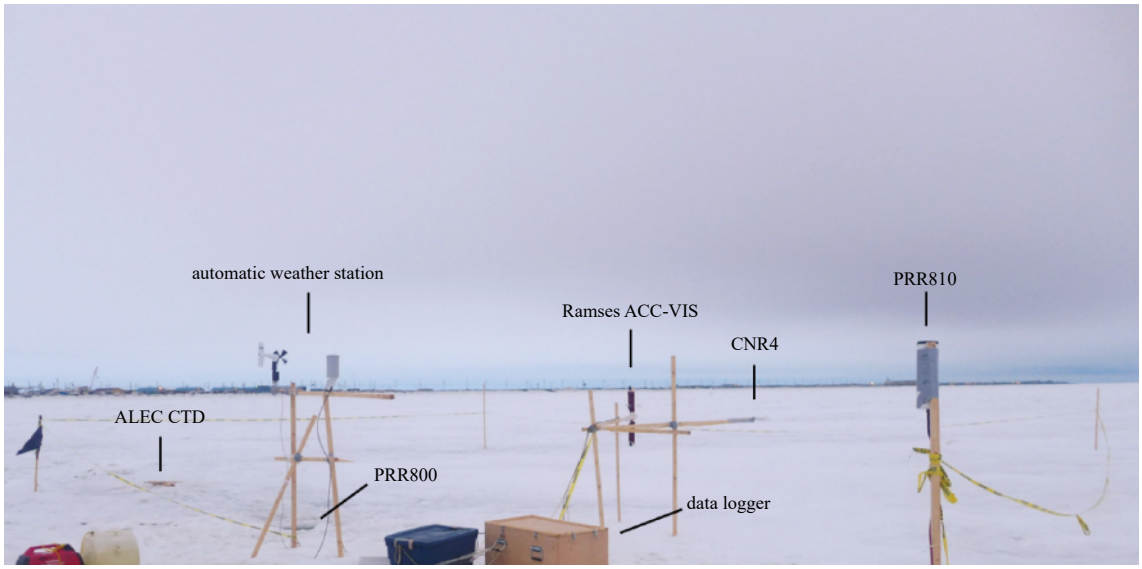

Fig. 3. *In situ* instrumentation on the site.

different instruments vary. In this study, $\delta(\lambda)$, determined by comparing multispectral instruments and hyperspectral instruments, is used to avoid overestimating E_s.

For sea ice with a thickness of H, the sum of the reflected energy, transmitted energy, and absorbed energy by the sea ice should be equal to the energy reaching the surface of the sea ice:

$$F_d(0,\lambda) = F_u(0,\lambda) + F_d(z,\lambda) + F_a(z,\lambda), \tag{5}$$

where $F_a(H, \lambda)$ is the energy absorbed by the sea ice. Dividing both sides of the equation by the incident radiation $F_d(0, \lambda)$, it becomes

$$1 = \alpha(\lambda) + T(H,\lambda) + A(H,\lambda), \tag{6}$$

where $A(H, \lambda)$ is the spectral absorbance of sea ice. Similarly, the integral absorbance of sea ice can be described as

$$A_t(H) = 1 - \alpha_t - T_t(H). \tag{7}$$

It can be seen from Eq. (7) that the absorbance of sea ice is related to the thickness of sea ice. Since the thickness of sea ice changed little during the 3-day observation period referenced in this paper, it can be concluded that the variation of sea ice absorbance was not related to the sea ice thickness.

As the valid bands differ between Ramses ACC and PRR800/810, spectral albedo and spectral transmittance cannot be compared directly. However, the average spectral resolution of the spectral albedo is 3.3 nm, which is much higher than that of the transmittance (31.7 nm). Therefore, the band of the spectral albedo was interpolated into an array at intervals of 1 nm, from which values at the same wavelengths as the spectral transmittance were selected to calculate the spectral absorbance of the sea ice.

2.3 *Radiative transfer model*

The solar radiation absorbed by sea ice is also closely related to the physical properties of the sea ice itself. Therefore, a two-stream radiative transfer model (Lu et al., 2016) was modified to study the effect of sea ice physical properties on albedo and transmittance. In the isotropic approach of this three-layer (snow, ice, and ocean) model, the inherent optical properties of each layer are defined by the wavelength-dependent scattering coefficient σ_λ and absorption coefficient k_λ. Under the assumption of diffuse incident solar radiation and isotropic scattering, the downwelling and upwelling irradiance at each layer are controlled by two coupled first-order differential equations:

$$\begin{cases} \mathrm{d}F^{\downarrow}(z,\lambda) = -k_\lambda F^{\downarrow}(z,\lambda)\mathrm{d}z - \sigma_\lambda F^{\downarrow}(z,\lambda) + \sigma_\lambda F^{\uparrow}(z,\lambda)\mathrm{d}z \\ \mathrm{d}F^{\uparrow}(z,\lambda) = k_\lambda F^{\uparrow}(z,\lambda)\mathrm{d}z + \sigma_\lambda F^{\uparrow}(z,\lambda) - \sigma_\lambda F^{\downarrow}(z,\lambda)\mathrm{d}z \end{cases}, \tag{8}$$

the solution of which is

$$\begin{cases} F^{\downarrow}(z,\lambda) = A(1-\mu_\lambda)\exp(\kappa_\lambda z) + B(1+\mu_\lambda)\exp(-\kappa_\lambda z) \\ F^{\uparrow}(z,\lambda) = A(1+\mu_\lambda)\exp(\kappa_\lambda z) + B(1-\mu_\lambda)\exp(-\kappa_\lambda z) \end{cases}, \tag{9}$$

where $\mu_\lambda = \sqrt{k_\lambda/(k_\lambda + 2\sigma_\lambda)}$ is the absorption strength ($\mu_\lambda = 0$ for purely scattering medium and $\mu_\lambda = 1$ for purely absorbing medium), $\kappa_\lambda = \sqrt{k_\lambda(k_\lambda + 2\sigma_\lambda)}$ is the attenuation coefficient, and A and B are constants determined by boundary conditions. Since there was always a wet snow layer on the surface, the reflection and scattering could not be distinguished. Therefore, the Fresnel reflection coefficient between air and snow was set to zero according to Perovich (1990).

The scattering coefficient and absorption coefficient of wet snow in the model are consistent with those defined in Perovich (1990). Because of the difference in the inclusions of fast ice in Barrow and floe ice in the central Arctic, the absorption caused by included particles and chlorophyll was also taken into account. The attenuation coefficients of sediment from Light et al. (1998) and those of chlorophyll from Mundy et al. (2007) were added to the radiative transfer model (Lu et al., 2016). The incident solar radiation, snow thickness, and ice thickness in the model were set to the averaged *in situ* value of one hour around 13:00, May 11.

3 Results and discussion

3.1 *Weather conditions*

Measurements were performed from May 1 to 14, 2014, with complete coverage of the automatic meteorological station and CNR4. Another two sets of instruments, PRR800/810 and Ramses ACC-VIS, collected data from May 10 to 12 with some interruptions due to precipitation. A time series of the air temperature, relative humidity, air pressure, and wind speed were recorded by the automatic weather station and are shown in Figs 4a–d. Since clouds have a significant impact on the amount of solar radiation that reaches the ice, the cloud cover over Barrow during the observation period was also recorded (Fig. 4e). From May 3 to 10, a low temperature of less than 0°C persisted for more than one week with a corresponding reduction of humidity and pressure. As a result, the snow on the surface of the sea ice did not melt until May 10, which kept the integral albedo higher than 0.8 during this period. Pressure reached its maximum of 1 017.9 hPa at 12:00 (all times are local time) on May 2 and then dropped to 986.6 hPa at 02:00 on May 4. It rose back to 1 011.1 hPa at around 0:00 on May 11. During the period of low pressure from May 3 to 9, the average temperature decreased from 1.43°C to –4.86°C, while the average wind speed increased from 1.72 m/s to 2.01 m/s. The average humidity ranged from 86.96% to 83.76% with a large variance from 17.91% to 53.74%. These values mean that the daily changes in the humidity were affected by the low pressure. After May 11, when the pressure returned to 1 009 hPa, the temperature rose back to 0.79°C, suggesting that the air temperature was significantly affected by the meteorological event. Cloud cover had an average value of 0.63 with a standard deviation of 0.30, making a significant factor affecting the incident solar radiation and the apparent optical properties of sea ice.

Because of the significant impact of the cloud coverage and precipitation on the apparent optical properties of fast ice, weather records at Barrow with high time resolution are shown in Table 1. As shown in Table 1, 12 h out of 72 h were recorded as "partly sunny", which means a clear sky was present for only 16.7% of the observation time. Cloudy weather accounted for 63.9% of the study period, and precipitation occurred during the remaining 19.4%. There were three periods of "light rain" at 10:00 and 23:00 on May 10 and at 13:00 on May 11. The rainy weather at these times interrupted instrument observations for 1–2 h. Two light rains at 23:00 on May 10 and 13:00 on May 11 caused significant changes in the surface state of the fast ice. Two abrupt changes in the albedo of the sea ice were recorded after resuming observations.

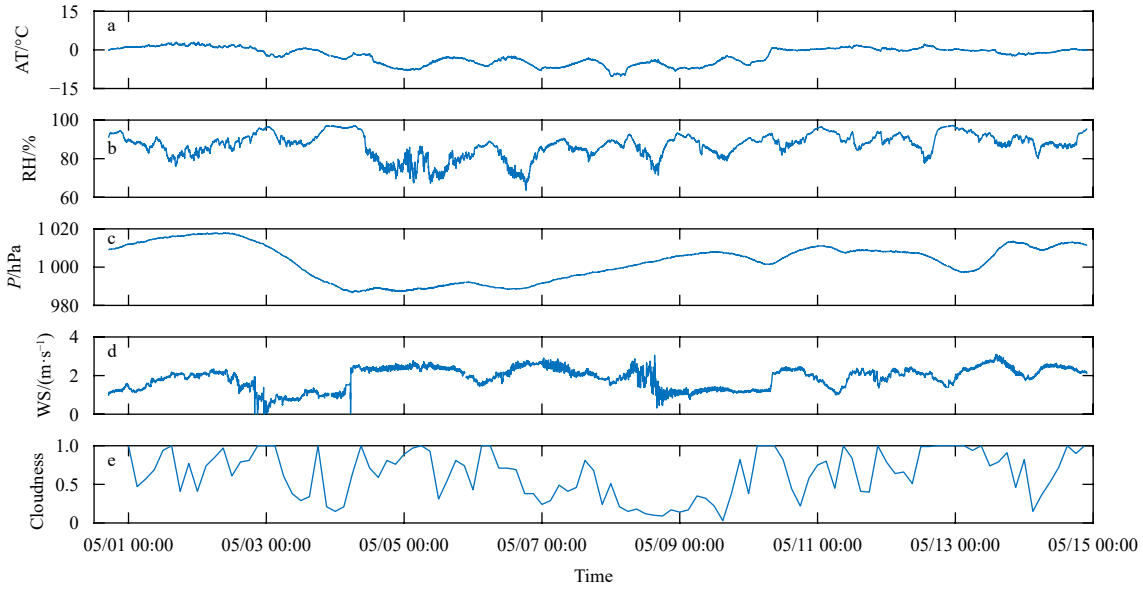

Fig. 4. Time series for air temperature (AT) (a), relative humidity (RH) (b), pressure (*P*) (c), wind speed (WS) (d), and cloudness (e) during the study period.

Table 1. Summary of the weather and sky conditions in Barrow

Time	Date		
	May 10	May 11	May 12
00:00	partly sunny	low clouds	scattered clouds
01:00	partly sunny	mostly cloudy	overcast
02:00	broken clouds	overcast	partly sunny
03:00	overcast	overcast	partly sunny
04:00	overcast	overcast	mostly cloudy
05:00	mostly cloudy	overcast	low clouds
06:00	light snow, ice fog	light rain, overcast	broken clouds
07:00	light snow, ice fog	overcast	broken clouds
08:00	light snow, mostly cloudy	overcast	low clouds
09:00	light freezing rain, vercast	mostly cloudy	low clouds
10:00	light rain, mostly cloudy	partly sunny	overcast
11:00	more clouds than sun	partly sunny	overcast
12:00	partly sunny	mostly cloudy	overcast
13:00	partly sunny	light rain, overcast	scattered clouds
14:00	partly sunny	mostly cloudy	scattered clouds
15:00	low clouds	overcast	partly sunny
16:00	low clouds	more clouds than sun	overcast
17:00	low clouds	overcast	mostly cloudy
18:00	low clouds	partly sunny	light rain, mostly cloudy
19:00	low clouds	scattered clouds	light snow, mostly cloudy
20:00	low clouds	passing clouds	light snow, mostly cloudy
21:00	low clouds	scattered clouds	light snow, more clouds than sun
22:00	partly sunny	passing clouds	light snow, overcast
23:00	drizzle, low clouds	broken clouds	light snow, ice fog

3.2 *Apparent optical properties*

3.2.1 *Albedo*

In the late spring, the solar radiation reaching the sea ice surface shows an obvious diurnal change, as shown in Fig. 5a. Using the 490 nm band as an example, the magnitude of shortwave radiation stays below 0.1 W/(m²·nm) from 18:00 in the afternoon to about 06:00 in the morning. Beginning at 06:00, R_{sd} gradually increases until 01:00, when the radiation energy reaches its daily maximum. Under differing weather conditions such as cloud cover, the magnitude of R_{sd} varies between 0.8 W/(m²·nm) and 1 W/(m²·nm). The diurnally changing pattern of R_{su} is basically the same as that of R_{sd}, which is a reduction in magnitude as shown in Fig. 5b. After the snowfall on May 11, values of R_{su} increased significantly, especially at noon, from 0.4 W/(m²·nm) on May 10 to around 0.6 W/(m²·nm) on May 11. Together with the small change in R_{sd} during these two days, the spectral albedo of the fast ice increased, and the absorbance decreased. In addition

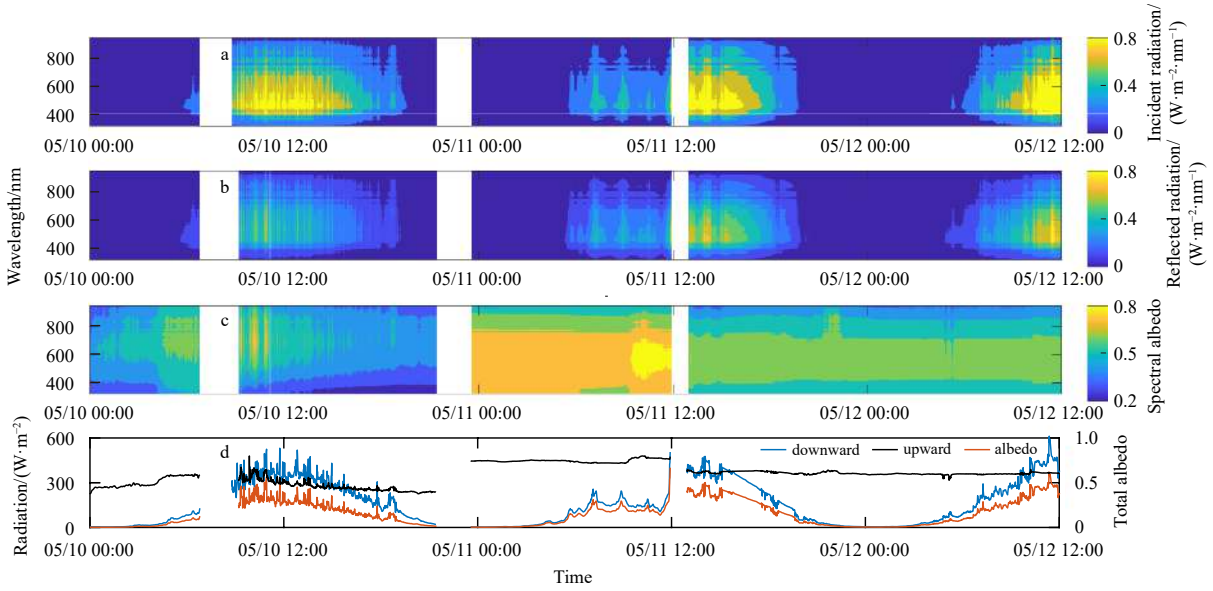

Fig. 5. Time series of the incident radiation (a), reflected radiation (b), spectral albedo (c), and integral albedo (d), measured by Ramses ACC-VIS in Barrow.

to the diurnal change, the incident and reflected radiation on the surface of the sea ice shows obvious differences in various spectral bands, especially at noon when the radiation reaches its peak as shown in Figs 5a and b. Most energy concentrates in the 450–550 nm band (blue and green light), while the amount of energy in the purple and red light band is relatively small.

For fast ice with thickness of 1.49 m, the spectral albedo is determined mainly by the surface condition of ice rather than the incident radiation. Therefore, the spectral albedo has no considerable diurnal change as shown in Fig. 5c. However, some abrupt changes in the albedo occurred after the rain or snow events. Combined with the weather conditions recorded in Table 1, the effect of precipitation on the surface albedo can be described as follows. For the sea ice covered by melting snow (before 0 am on May 11), the albedo increased along with the wavelength. After snowfall, the albedo of the sea ice rose significantly (even before dawn when the incident radiation is very small), with a maximum appearing in the blue-green band around 550 nm. At 12:00 on May 11, drizzle caused an overall decrease in the albedo of sea ice, while its variation trend remained stable with wavelength.

The temporal variation of the spectral albedo basically represents the characteristics of the integrated albedo, which is shown in Fig. 5d. From May 10 to 12, the integral albedo of the sea ice varied between 0.33 and 0.79. Before the snowfall at 0:00 on May 11, the surface of the sea ice was covered by melting snow with an integrated albedo of 0.44. When the melting snow was covered by dry snow after the snowfall, the albedo of the sea ice increased rapidly up to 0.75, which reflects the characteristics of fresh snow. With the arrival of drizzle at 12:00 on May 11, the dry snow started to melt due to the solar radiation heating, which made the surface albedo decrease to 0.62. Since the thickness of snow on the surface of sea ice increased, the value of the albedo at this time varied between 0.44 and 0.75. Perovich and Polashenski (2012) analyzed four long-term observations of sea ice albedo near Barrow and found that the sea ice albedo in 2000 and 2001 was 0.8 before May 29, then gradually decreased to 0.6 when melt ponds appeared, and then declined further to about 0.3. The changes of albedo in 2008 and 2009 were the same, but the date that melt started advanced to May 10, which made the declining rate of albedo in 2009 significantly faster than in 2008. The results show that the melting date of the sea ice in 2014 along the Barrow coast advanced even further. On May 9, the snow on the surface of the sea ice had begun to melt, and the albedo had decreased to about 0.5. The continuous increase in local temperature since 2000 has caused sea ice to melt earlier. However, snowfall in spring will significantly affect the albedo of sea ice before melt ponds form.

3.2.2 *Transmittance*

Observation of sea ice transmission began at 10:00 on May 10 and ended at around 13:30 on May 12. Similar to the pattern seen in albedo, the incident radiation measured by the PRR800/810 revealed significant diurnal variations with a maximum at around 01:00 as shown in Fig. 6a. The change of incident radiant energy is dependent on the spectrum with a maximum value of 450–550 nm and a magnitude of 1 W/(m²·nm). Only a small amount of radiation was left after the solar energy transmitted through 1.49 m of melting sea ice. The transmitted radiation has revealed a diurnal change (Fig. 6b) with a maximum record of 8×10^{-3} W/(m²·nm) at 550 nm.

In spite of the significant diurnal changes in both incident and transmitted radiation, the transmittance depends mainly on the properties of sea ice, which is also the case for albedo. Consequently, there is no diurnal variation in the transmittance of sea ice as shown in Fig. 6c. The spectral transmittance reaches its maximum of about 0.01 at 550–580 nm, and decreases gradually toward both sides of the spectrum. Radiation transferred through the 1.49 m of melting ice accounts for only 1% of the incident energy on the ice surface, even for the band with the strongest transmission capability. This means that 99% of the incident energy is reflected and absorbed by the sea ice. During the observations, the thickness of the ice thinned by only 1 cm over three days as the sea ice melted. However, this small reduction in thickness still increased the integral transmittance from 0.001 3 to 0.004 1, as shown in Fig. 6d. The low magnitude of integral

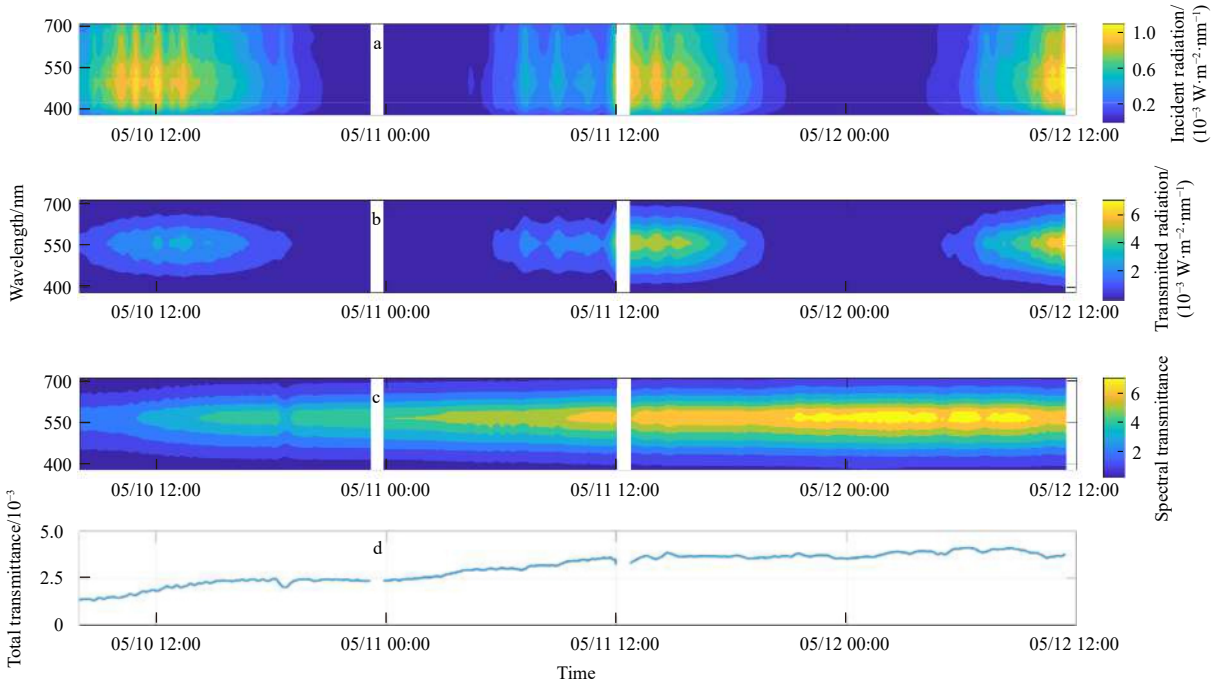

Fig. 6. Time series of the incident radiation (a), transmitted radiation (b), spectral transmittance (c), and integral transmittance (d), measured by PRR800/810 in Barrow.

transmittance in this observation (0.002 8 on average) is consistent with previous studies (between 0.002 and 0.003) on sea ice in May (Nicolaus et al., 2010, 2013; Katlein et al., 2019). During this period, the transmittance was influenced mainly by sea ice thickness and had no obvious relationship with precipitation or surface conditions.

3.2.3 *Absorbance*

According to Eq. (5), the solar radiation absorbed by sea ice can be derived from the incident, reflected, and transmitted radiation. From the results in Section 3.2.2, the transmittance is less than 0.01, which means that less than 1% of the incident energy enters the sea water under ice. Therefore, most of the incident energy reaching the surface was reflected and absorbed by the sea ice, causing an opposite change on its absorbance and albedo. Before snowfall on May 11, the albedo of the melting snow was relatively low, while the energy absorbed by the sea ice (450–550 nm) was around 0.5 W/(m²·nm), as shown in Figs 7a and b. After snowfall, the albedo reached more than 0.8, which means that most of the solar radiation was reflected back into the atmosphere, reducing the absorbed energy to 0.1 W/(m²·nm). Due to the melting of dry snow on the surface and drizzle that occurred at noon on May 11, the albedo decreased causing the energy absorbed by the fast ice to increase to 0.3 W/(m²·nm).

Based on Eq. (6), the spectral absorbance of sea ice is closely related to spectral albedo and transmittance. Due to the thickness and melting stage of the sea ice, the spectral transmittance was extremely low (0.01). Therefore, the spectral absorbance and albedo had a strong negative correlation. Before the snowfall, the sea ice had a better absorption capacity at the shorter wavelengths, as shown in Fig. 7c. With the surface of sea ice covered by dry snow, the spectral absorbance rapidly decreased to 0.2 with a weak variation in wavelengths. As the fresh snow melted, the spectral absorbance increased gradually without any change in wavelengths. Combining the wavelength-integrated albedo and transmittance, the integral absorbance of sea ice can be obtained as shown in Fig. 7c. Before snowfall, the absorption rate of the sea ice varied from 0.39 to 0.61, increasing as the wavelengths decreased. Meanwhile, the absorbance of the sea ice had an overall rising trend, which means that the absorption capacity of the sea ice was increasing. After snowfall, more incident radiation was reflected, resulting in a rapid reduction in absorbance to about 0.2. As the dry snow on the surface melted, the solar radiation absorption capacity of the sea ice increased to 0.3 and ultimately to 0.39 by the end of the observation period.

From the results above, it can be concluded that solar radiation absorption and reflection have a significant negative correlation for thick fast ice in the melting season due to the lower transmittance of less than 0.005, which means that the absorbed energy decreases as the reflected radiation increases, and vice versa.

3.3 *Energy balance on the surface of the fast ice*

Energy balance on the sea ice surface can be written as follows (Persson et al., 2002; Else et al., 2014):

$$F_{\mathrm{net}} = R_{\mathrm{sd}} + R_{\mathrm{su}} + R_{\mathrm{ld}} + R_{\mathrm{lu}} + F_{\mathrm{sp}} + F_{\mathrm{ep}} + G, \tag{10}$$

where F_{net} is the total heat flux of the sea ice surface, R_{sd} is shortwave incident radiation, R_{su} is shortwave reflected radiation, R_{ld} is longwave incident radiation, R_{lu} is longwave reflected radiation, F_{sp} is sensible heat flux, F_{ep} is latent heat flux, and G is the subsurface heat conduction.

3.3.1 *Turbulent heat flux*

The observations of the fast ice were carried out in the late spring and early summer, during the initial stage of sea ice melting. The melting of sea ice generally proceeds from the surface to the interior. The main source of heat for melting is solar radiation on the surface, advection of seawater under the ice bottom,

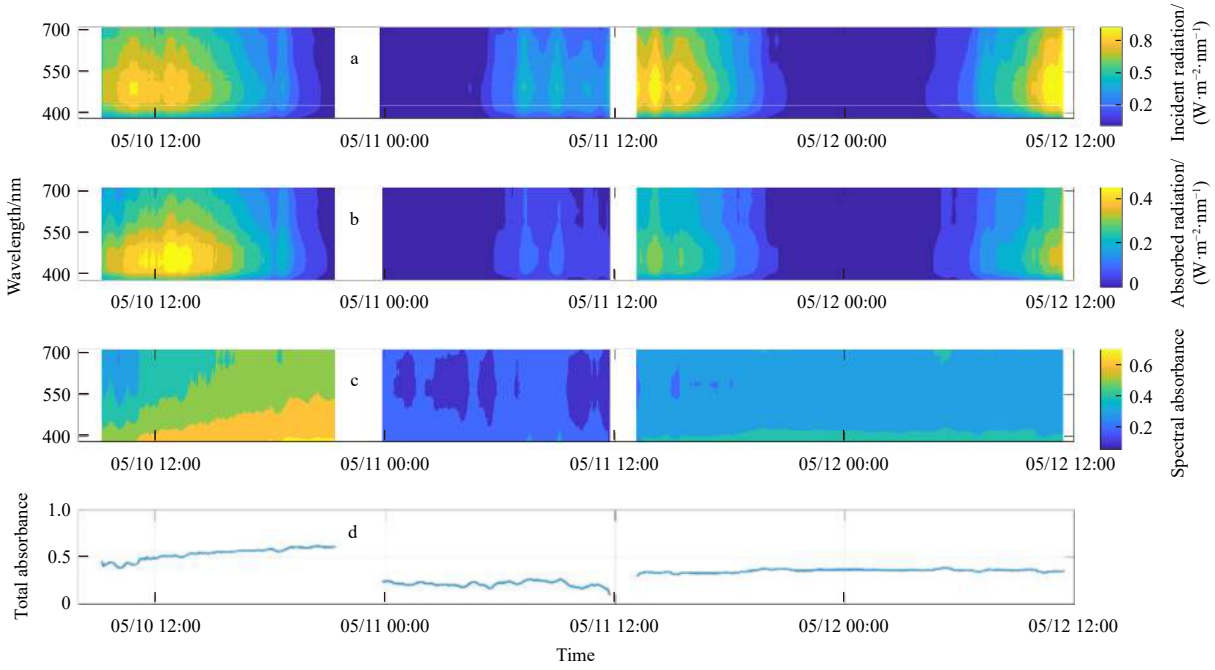

Fig. 7. Time series of the incident radiation (a), absorbed radiation (b), spectral absorbance (c), and integral absorbance (d), derived from interpolated data from Ramses ACC-VIS and PRR800/810 in Barrow.

and the heat conducted from the bottom into the interior. For seasonal fast ice, the heat for sea ice melting comes mainly from solar radiation. Advection heating makes little contribution to melting due to the distance from the ocean's interior.

In this study, a time series of the surface radiation flux over 14 days was obtained (Figs 8a and b) using the CNR4 to measure the incident and reflected radiation in both shortwave and longwave bands. Based on the air temperature, air pressure, relative humidity, and wind speed measured by the automatic weather station, surface heat flux was derived as follows (Fig. 8c).

Sensible heat flux (F_{sp}) and latent heat flux (F_{ep}) can be calculated as in Maykut (1978, 1982)

$$F_{sp} = \rho_a c_p C_s u \left(T_a - T_w\right), \tag{11}$$

$$F_{ep} = 0.622 \rho_a L_v C_e u \left(re_{sa} - e_{sw}\right) / P, \tag{12}$$

where ρ_a is the air density, c_p is the specific heat of air, C_s is the

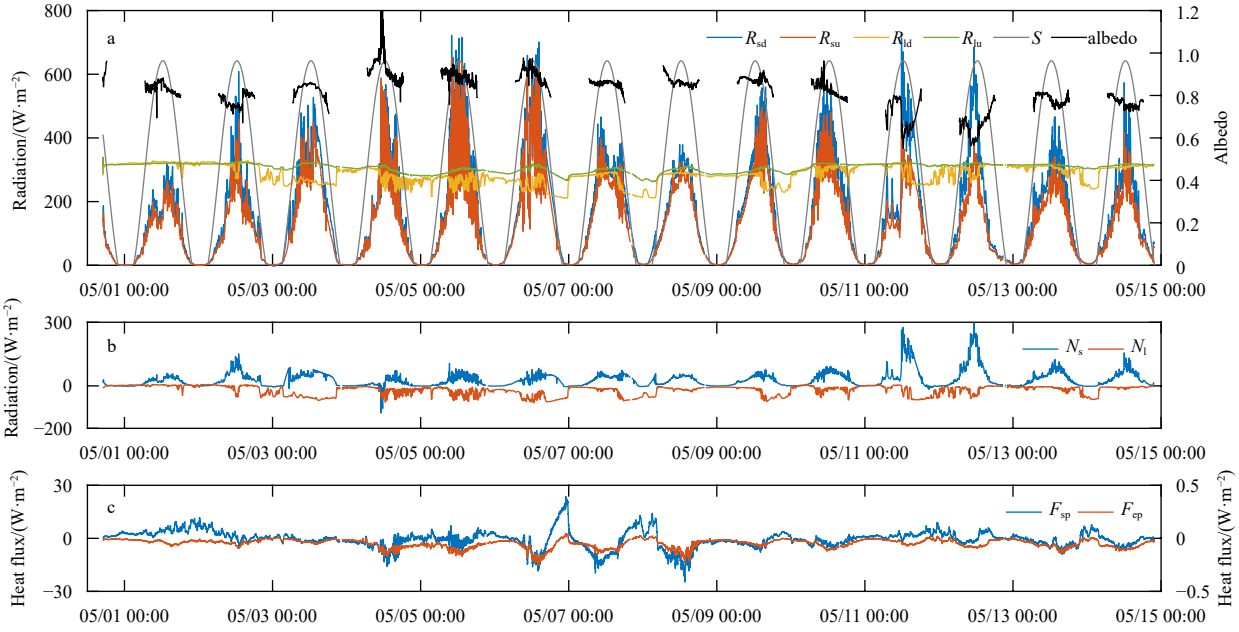

Fig. 8. Variations in radiation and heat flux on the surface of the fast ice, including the incident shortwave R_{sd}, reflected shortwave R_{su}, incident longwave R_{ld}, reflected longwave R_{lu}, solar radiation at top of the atmosphere S, and albedo (a), net shortwave and longwave radiation (N_s and N_l) (b), and turbulent heat flux (c). The y-axis on the right in panel c is for the latent heat flux F_{ep}.

transfer coefficient for sensible heat, T_a is the air temperature, T_w is the surface temperature, L_v is the latent heat of vaporization, C_e is the transfer coefficient for latent heat, P is the surface pressure, e_{sa} is the air saturation vapor pressure, e_{sw} is the surface saturation vapor pressure, u is the wind speed, and r is the relative humidity, given that ρ_a=1.29 kg/m^3, c_p=1 030 J/(kg·K), C_s=C_e=1.75×10^{-3}, and L_v=2.49×10^6 J/kg.

During the observation period, sun at Barrow was below the horizon only for 2–3 h a day. The shortwave radiation showed a significant diurnal change while it was always smaller than the theoretical value of reaching the top of the atmosphere due to the cloudiness. Cloud cover also had an effect on the peak value of shortwave radiation at noon. The peak value of incident shortwave radiation with high cloud cover (May 12–14) was significantly smaller than that when the cloud cover was low (May 8–9). Solar radiation during the two periods mentioned above had relatively low fluctuation at noon. Given the uncertainty in CRN4 albedo measurements when the solar altitude angle is low, only the albedo at altitude angles greater than 10° is discussed. As can be seen from Fig. 8a, the integral albedo was about 0.75 from May 1 to 3, and then increased to 0.85 on May 4, remaining in the range of 0.8–0.85 until May 11. After that, the albedo rapidly declined to 0.7 and reached a minimum value of 0.57 at noon on May 11 and 12. The albedo obviously responded to the change in air temperature, as can be seen in Figs 8a and 4. The temperature was higher than 0°C from May 1 to 3 and May 11 to 15, and below 0°C from May 4 to 10. At low temperatures, the dry snow maintained an albedo above 0.8. As the air temperature rose, the snow cover started to melt, which in turn lead to a decrease in albedo. The precipitation on May 11 also had a significant effect on the albedo. The drizzle at 13:00 made the snow on the surface wet, so the albedo reached a low of 0.57. After the precipitation, the albedo rose to 0.78 as the surface refroze due to the low temperature.

The net shortwave radiation N_s was positive during the entire observation period, reaching a peak of 296.74 W/m^2 on May 11 and 12. At other times, N_s was less than 100 W/m^2, depending on the shortwave incident radiation and albedo. Since cloud cover has a relatively small effect on shortwave incident radiation, it can be concluded that albedo is the decisive factor for net shortwave radiation. Compared with N_s, the net longwave radiation N_l was negative throughout the observation period with a minimum value of –79.69 W/m^2. Its magnitude was determined mainly by the large variation in longwave downward radiation (Fig. 8a).

There was a significant disparity in magnitude between the latent heat flux and the sensible heat flux on the ice surface, as shown in Fig. 8c. While the surface of the sea ice in summer is covered by melt ponds, in the spring a snow-covered surface is common. Therefore, the latent heat flux in spring is extremely small, and the sensible heat flux caused by the difference in temperature is the major component of the turbulent heat flux. The sensible heat flux reached a maximum value of 23.7 W/m^2 at 23:00 on May 7, which was due to the high wind speed and surface temperature difference at that time. The maximum value of latent heat flux (0.04 W/m^2) occurring at the same time was caused by the maximum of wind speed and the minimum of relative humidity. The average values of sensible heat flux and latent heat flux were –0.431 W/m^2 and –0.044 W/m^2, respectively. By comparing the magnitude of the net shortwave radiation and net longwave radiation, it can be seen that the sea ice shows no trend of gaining or losing energy through turbulent heat flux on the surface. Therefore, the sea ice lost energy through the net longwave radiation as the net shortwave radiation became its main heating source.

3.3.2 *Heat conduction*

According to Liu et al. (2020), the heat conduction of sea ice with snow cover can be written as

$$G = -k_s \frac{T_s - T_{ice}}{d_s}, \tag{13}$$

where k_s=0.3 W/(m·°C) is the thermal conductivity of snow, T_s is the snow surface temperature, T_{ice} is the ice surface temperature, and d_s is the snow thickness. An ice core was sampled on site at 06:00 on May 11, at which time the surface temperatures of the ice and the snow (–2.21°C and 0.42°C, respectively) were measured as well as the snow thickness (5 cm).

At the moment the ice core was measured, the sea ice was gaining energy as shortwave radiation and losing energy as longwave radiation with an order of magnitude difference (Fig. 9), which is consistent with the energy budget in Section 3.3.1. In addition, the sensible heat flux on the surface was positive but small, since the snow surface temperature (0.423°C) was close to the air temperature (0.524°C). The latent heat flux was negative with an extremely minimum value, almost negligible when compared to other terms in an equation. The results also show that heat conduction to the surface was in a negative status, which meant the sea ice was losing energy through heat conduction to the surface. The heat conduction had a value of about half the net shortwave radiation, accounting for 81.2% of the total energy loss. Although heat conduction with relatively more energy loss was considered, net heat flux F_{net} according to Eq. (10) was positive with a value of 14 W/m^2. Therefore, the addition of a heat conduction term will not change the general trend of sea ice melting in spring. The results above show that heat conduction plays an important role in the energy budget of sea ice and has a positive correlation with temperature difference inside the sea ice. Therefore, in the spring, variations in the snow temperature caused by air temperature or surface state will significantly change the value of heat conduction, which in turn affects the rate of ice melting.

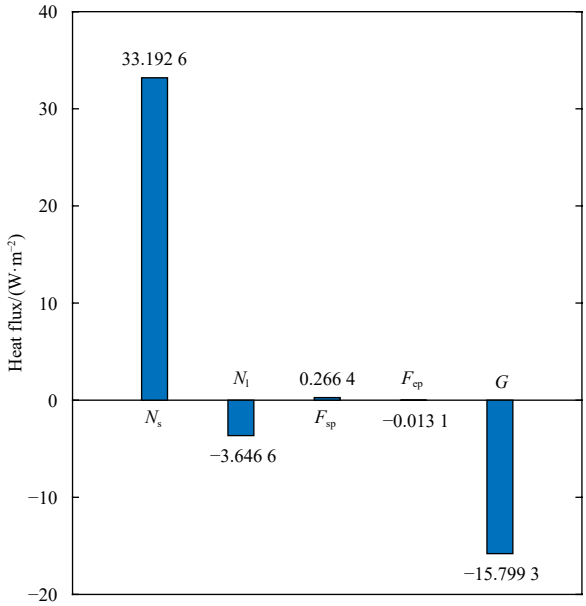

Fig. 9. Energy budget of fast ice in the spring. From left to right: net shortwave radiation, net longwave radiation, sensible heat flux, latent heat flux, and heat conduction, with their values marked.

3.4 *Impact of inclusions in the fast ice on the optical properties*

A main difference between pack ice and fast ice is the amount of inclusions, which significantly influence the optical properties of the ice. To quantify the impact of sea ice inclusions, the radiative transfer model modified in Section 2.3 was used to simulate the spectral albedo and spectral transmittance of sea ice. The model is based on the surface state of sea ice (wet snow at that time) after light rain at 13:00 on May 11. Therefore, the surface incident radiation was set to the average value of one hour before and after 13:00 on May 11. The ice thickness and the snow depth were set to measured values of that day, which were 144 cm and 2 cm, respectively. Although the effects of inclusions such as particulates on the albedo of sea ice depend to a large degree on their vertical distribution within the ice (Light et al., 1998), the influence of particulate impurities on the overall scattering of sea ice can be negligible (Ehn et al., 2008b). Besides, there are few studies on the dependence of transmittance on the vertical distribution of sea ice inclusions. Therefore, in the radiative transfer model used in this study, the particulate matter and chlorophyll within sea ice are assumed to be evenly distributed vertically.

In the model results (Fig. 10a) obtained under the described conditions, the simulated albedo agrees well with field measurements. According to the observations and weather records, the snow layer on the surface of the sea ice was affected by the rain at 11:00–12:00 on May 11, changing from dry snow to wet snow. Therefore, the integral albedo fell from 0.76 to 0.63 with the peak value of spectral albedo appearing near 600 nm. Compared with the *in situ* measurements, the simulated spectral albedo decreased monotonically from 400 nm to 950 nm. The reason for the decrease is that the effects of particulate matter on the spectral albedo were not taken into account when setting the surface parameters for the model (Light et al., 1998; Ehn et al., 2008b). Light et al. (1998) found that as the concentration of sediments increased, the albedo at each wavelength decreased, while the peak shifted from 450 nm for clean ice to around 550 nm. However, the model including a sediment-laden ice layer below the surface did not show the same result on the position of the peak, which can be considered as the effect of snow on the surface. For fast ice with snow about 2 cm thick, the albedo is basically determined by the scattering and absorption coefficients of the surface layer with a weak effect from the underlying ice, consistent with the minor decrease on the spectrum peak for the sea ice with inclusion.

Another impact of the inclusions in the ice on the optical properties is to alter the magnitude and spectrum shape of the absorbed and transmitted radiation as shown in Fig. 10b. Maximum values of the transmittance from the *in situ* observations and simulations with and without the inclusions in the ice reached 0.006 4, 0.006 0, and 0.071, which shows a 10 times overestimation without regard to the interior inclusions (Fig. 10b). Moreover, the peak value in wavelength in the model without particulate matter or biomass appears around 450 nm, which is 100 nm smaller than observed in the field. Based on the *in situ* measurements, simulated particulate matter content is estimated at 95.78 g/m^2 with a chlorophyll concentration of 5.51 mg/m^2.

The disparity between the two peak values of simulated and observed transmittance is caused by the difference in the composition of included particles in the fast ice and the floe (Nürnberg et al., 1994; Stierle and Eicken, 2002). The *in situ* ice core sampling from the surface to 70 cm depth (Fig. 11) showed obviously visible particles in the middle of the ice. For visually discolored ice, the content of particle matter is between 100 g/m^2 and 200 g/m^2 (Osterkamp and Gosink, 1984; Kempama et al., 1989; Reimnitz et al., 1993; Eicken et al., 1997, 2005; Gradinger et al., 2009), which is consistent with the simulation result of 95.78 g/m^2. Particulate matter also affects algal growth in the spring by modulating the available light intensities. According to Gradinger et al. (2009), chlorophyll concentrations in the spring at Barrow can reach 36 mg/m^2 in clean ice and 1 mg/m^2 in sediment-laden ice, of which the particulate matter content were 6 g/m^2 and 106 g/m^2, respectively. In this study, the spring bloom of ice algae was retarded due to the reduction of transmitted light, so the chlorophyll reached only 5.51 mg/m^2. This is higher than the result of Gradinger et al. (2009) and closer to the obser-

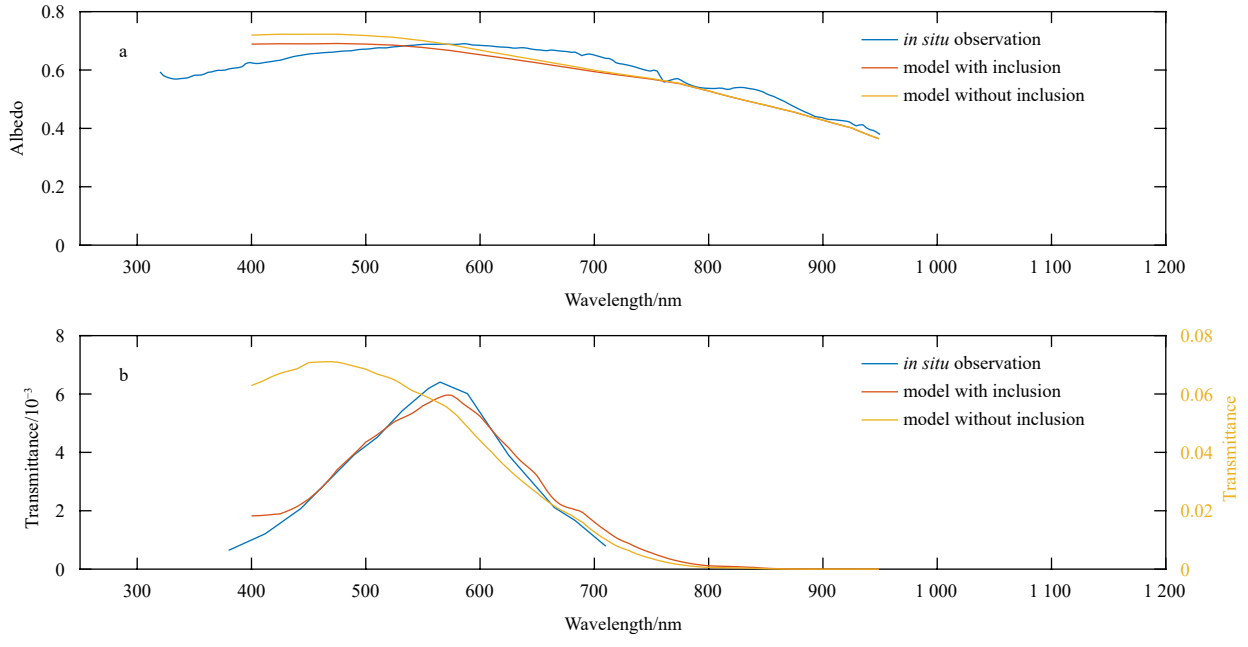

Fig. 10. Spectrum-independence of the albedo (a) and transmittance (b) from *in situ* observations and simulations with and without inclusions in the ice. The *y*-axis on the right in panel b is for the curve without interior inclusions.

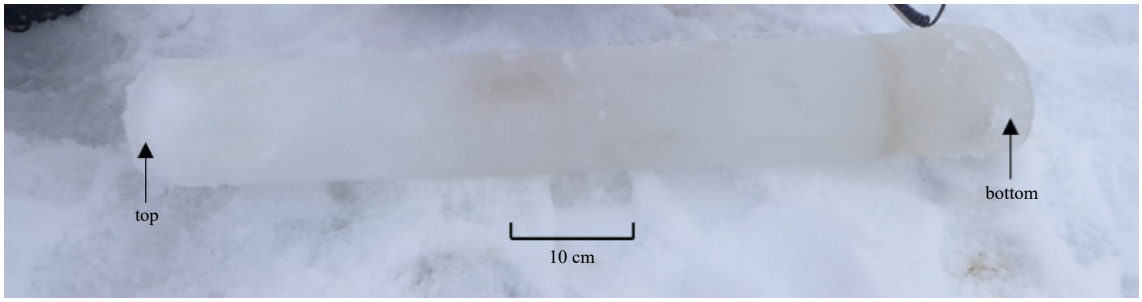

Fig. 11. Upper part of the ice core sampled at the site in Barrow.

vation of Nicolaus et al. (2013) at the same location in May 2010 (3 mg/m^2).

4 Conclusions

A quantification of the optical properties and energy budget of sea ice in spring was developed based on the observations of land-fast ice in Barrow in May of 2014. The effect of particulate matter and biomass on the transmittance of sea ice was simulated using a two-stream radiative transfer model.

In this study, the start date of sea ice melting advanced to earlier than May. Before the melt ponds form, both precipitation and air temperature affect the snow cover on the surface of the sea ice, resulting in repeated changes in the albedo between 0.85 and 0.57. During the observation period, the temperature dropped from 1.43°C to –4.86°C due to the presence of a low pressure system for one week (May 3–10), increasing the albedo up to 0.89. In addition, on May 11, the albedo rose from 0.44 to 0.75 due to snow at 0:00, and then reduced to 0.62 after the drizzle at 12:00.

The absorbance of the fast ice changed between 0.22 and 0.61 as the transmittance rose from 1.3×10^{-3} to 4.1×10^{-3} from May 10 to May 12. Because the transmittance of the fast ice was less than 0.01 during the observation period, a negative correlation between albedo and absorbance can be clearly established. However, the transmittance of sea ice varies only with time, showing a one-fold increase in all bands over two days. No obvious relationship with surface condition was found.

The values of sensible and latent heat flux for the fast ice averaged only –0.431 W/m^2 and –0.044 W/m^2, respectively, showing no significant trend. Sea ice at this stage loses energy mainly through net longwave radiation and gains energy through net shortwave radiation. Heat conduction plays an important role in the energy budget of sea ice in the spring, accounting for 81.2% of the energy loss. However, in May sea ice still gains energy overall. The value of the heat conduction reaches –15.79 W/m^2, nearly half the value of the net shortwave radiation. Since heat conduction is positively correlated with the temperature difference between the ice layer and the snow layer, the variations in air temperature or surface condition can affect the heat conduction, further altering the rate of sea ice melting.

The numerical simulation results show that in the spring, the albedo of the fast ice is determined mainly by the thickness and optical properties of snow on the surface, while the transmittance is affected by the snow depth, sea ice thickness, and amount of inclusions. Among these factors, the effect of snow depth on the transmittance is the most significant, which is in consistent with previous research. Concentrations of the chlorophyll and particulate matter inclusions were estimated at 5.51 mg/m^2 and 95.78 g/m^2. These inclusions significantly affect the magnitude and distribution of the spectral albedo and transmittance. Therefore, the physical and biological sampling of ice cores in the field is necessary to evaluate the optical properties of sea ice and further improve the radiative transfer model.

References

Barber D G, Asplin M G, Raddatz R L, et al. 2012. Change and variability in sea ice during the 2007–2008 Canadian International Polar Year program. Climatic Change, 115(1): 115–133, doi: 10.1007/s10584-012-0477-6

Barber D G, Galley R, Asplin M G, et al. 2009. Perennial pack ice in the southern Beaufort Sea was not as it appeared in the summer of 2009. Geophysical Research Letters, 36(24): L24501, doi: 10.1029/2009GL041434

Campbell K, Mundy C J, Barber D G, et al. 2014. Remote estimates of ice algae biomass and their response to environmental conditions during spring melt. Arctic, 67(3): 375–387, doi: 10.14430/arctic4409

Comiso J C. 2012. Large decadal decline of the Arctic multiyear ice cover. Journal of Climate, 25(4): 1176–1193, doi: 10.1175/JCLI-D-11-00113.1

Comiso J C, Parkinson C L, Gersten R, et al. 2008. Accelerated decline in the Arctic sea ice cover. Geophysical Research Letters, 35(1): L01703, doi: 10.1029/2007GL031972

Ehn J K, Mundy C J, Barber D G. 2008a. Bio-optical and structural properties inferred from irradiance measurements within the bottommost layers in an Arctic landfast sea ice cover. Journal of Geophysical Research: Oceans, 113(C3): C03S03, doi: 10.1029/2007jc004194

Ehn J K, Papakyriakou T N, Barber D G. 2008b. Inference of optical properties from radiation profiles within melting landfast sea ice. Journal of Geophysical Research: Oceans, 113(C9): C09024, doi: 10.1029/2007jc004656

Eicken H, Gradinger R, Gaylord A, et al. 2005. Sediment transport by sea ice in the Chukchi and Beaufort Seas: increasing importance due to changing ice conditions?. Deep-Sea Research Part II: Topical Studies in Oceanography, 52(24–26): 3281–3302, doi: 10.1016/j.dsr2.2005.10.006

Eicken H, Reimnitz E, Alexandrov V, et al. 1997. Sea-ice processes in the Laptev Sea and their importance for sediment export. Continental Shelf Research, 17(2): 205–233, doi: 10.1016/S0278-4343(96)00024-6

Else B G T, Papakyriakou T N, Raddatz R, et al. 2014. Surface energy budget of landfast sea ice during the transitions from winter to snowmelt and melt pond onset: the importance of net longwave radiation and cyclone forcings. Journal of Geophysical Research: Oceans, 119(6): 3679–3693, doi: 10.1002/2013JC009672

Gerland S, Haas C, Nicolaus M, et al. 2004. Seasonal development of structure and optical surface properties of fast ice in Kongsfjorden, Svalbard. Bremerhaven, Germany: Alfred Wegener Institute for Polar & Marine Resecareh, 26–34

Gerland S, Winther J G, Ørbæk J B, et al. 1999. Physical properties, spectral reflectance and thickness development of first year fast ice in Kongsfjorden, Svalbard. Polar Research, 18(2): 275–282,

doi: 10.3402/polar.v18i2.6585
Gradinger R R, Kaufman M R, Bluhm B A. 2009. Pivotal role of sea ice sediments in the seasonal development of near-shore Arctic fast ice biota. Marine Ecology Progress Series, 394: 49–63, doi: 10.3354/meps08320
Grenfell T C, Light B, Perovich D K. 2006. Spectral transmission and implications for the partitioning of shortwave radiation in arctic sea ice. Annals of Glaciology, 44: 1–6, doi: 10.3189/172756406781811763
Grenfell T C, Perovich D K. 1984. Spectral albedos of sea ice and incident solar irradiance in the southern Beaufort Sea. Journal of Geophysical Research: Oceans, 89(C3): 3573–3580, doi: 10.1029/JC089iC03p03573
Grenfell T C, Perovich D K. 2004. Seasonal and spatial evolution of albedo in a snow-ice-land-ocean environment. Journal of Geophysical Research: Oceans, 109(C1): C01001, doi: 10.1029/2003jc001866
Grenfell T C, Perovich D K, Eicken H, et al. 2007. Energy-and mass-balance observations of the land-ice-ocean-atmosphere system near Barrow, Alaska, USA, November 1999–July 2002. Annals of Glaciology, 44: 193–199, doi: 10.3189/172756406781811222
Grenfell T C, Warren S G. 1999. Representation of a nonspherical ice particle by a collection of independent spheres for scattering and absorption of radiation. Journal of Geophysical Research: Atmospheres, 104(D24): 31697–31709, doi: 10.1029/1999JD900496
Haas C, Pfaffling A, Hendricks S, et al. 2008. Reduced ice thickness in Arctic transpolar drift favors rapid ice retreat. Geophysical Research Letters, 35(17): L17501, doi: 10.1029/2008GL034457
Hamre B, Winther J G, Gerland S, et al. 2004. Modeled and measured optical transmittance of snow-covered first-year sea ice in Kongsfjorden, Svalbard. Journal of Geophysical Research: Oceans, 109(C10): C10006, doi: 10.1029/2003jc001926
Hudson S R. 2011. Estimating the global radiative impact of the sea ice-albedo feedback in the Arctic. Journal of Geophysical Research: Atmospheres, 116(D16): D16102, doi: 10.1029/2011JD015804
Katlein C, Arndt S, Belter H J, et al. 2019. Seasonal evolution of light transmission distributions through Arctic sea ice. Journal of Geophysical Research: Oceans, 124(8): 5418–5435, doi: 10.1029/2018JC014833
Kempama E W, Reimnitz E, Barnes P W. 1989. Sea ice sediment entrainment and rafting in the Arctic. Journal of Sedimentary Research, 59(2): 308–317
Kwok R, Rothrock D A. 2009. Decline in Arctic sea ice thickness from submarine and ICESat records: 1958–2008. Geophysical Research Letters, 36(15): L15501, doi: 10.1029/2009GL039035
Leu E, Mundy C J, Assmy P, et al. 2015. Arctic spring awakening-steering principles behind the phenology of vernal ice algal blooms. Progress in Oceanography, 139: 151–170, doi: 10.1016/j.pocean.2015.07.012
Light B, Eicken H, Maykut G A, et al. 1998. The effect of included particulates on the spectral albedo of sea ice. Journal of Geophysical Research: Oceans, 103(C12): 27739–27752, doi: 10.1029/98jc02587
Light B, Grenfell T C, Perovich D K. 2008. Transmission and absorption of solar radiation by Arctic sea ice during the melt season. Journal of Geophysical Research: Oceans, 113(C3): C03023, doi: 10.1029/2006jc003977
Light B, Perovich D K, Webster M A, et al. 2015. Optical properties of melting first-year Arctic sea ice. Journal of Geophysical Research: Oceans, 120(11): 7657–7675, doi: 10.1002/2015JC011163
Liu Changwei, Gao Zhiqiu, Yang Qinghua, et al. 2020. Measurements of turbulence transfer in the near-surface layer over the Antarctic sea-ice surface from April through November in 2016. Annals of Glaciology, 61(82): 12–23, doi: 10.1017/aog.2019.48
Lu Peng, Leppäranta M, Cheng Bin, et al. 2016. Influence of melt-pond depth and ice thickness on Arctic sea-ice albedo and light transmittance. Cold Regions Science and Technology, 124: 1–10, doi: 10.1016/j.coldregions.2015.12.010
Malinka A, Zege E, Heygster G, et al. 2016. Reflective properties of white sea ice and snow. The Cryosphere, 10(6): 2541–2557, doi: 10.5194/tc-10-2541-2016
Markus T, Stroeve J C, Miller J. 2009. Recent changes in Arctic sea ice melt onset, freezeup, and melt season length. Journal of Geophysical Research: Oceans, 114(C12): C12024, doi: 10.1029/2009JC005436
Maslanik J A, Fowler C, Stroeve J, et al. 2007. A younger, thinner Arctic ice cover: increased potential for rapid, extensive sea-ice loss. Geophysical Research Letters, 34(24): L24501, doi: 10.1029/2007GL032043
Maslanik J, Stroeve J, Fowler C, et al. 2011. Distribution and trends in Arctic sea ice age through spring 2011. Geophysical Research Letters, 38(13): L13502, doi: 10.1029/2011GL047735
Maykut G A. 1978. Energy exchange over young sea ice in the central Arctic. Journal of Geophysical Research: Oceans, 83(C7): 3646–3658, doi: 10.1029/JC083iC07p03646
Maykut G A. 1982. Large-scale heat exchange and ice production in the Central Arctic. Journal of Geophysical Research: Oceans, 87(C10): 7971–7984, doi: 10.1029/JC087iC10p07971
Mundy C J, Ehn J K, Barber D G, et al. 2007. Influence of snow cover and algae on the spectral dependence of transmitted irradiance through Arctic landfast first-year sea ice. Journal of Geophysical Research: Oceans, 112(C3): C03007, doi: 10.1029/2006JC003683
Nghiem S V, Rigor I G, Perovich D K, et al. 2007. Rapid reduction of Arctic perennial sea ice. Geophysical Research Letters, 34(19): L19504, doi: 10.1029/2007GL031138
Nicolaus M, Gerland S, Hudson S R, et al. 2010. Seasonality of spectral albedo and transmittance as observed in the Arctic Transpolar Drift in 2007. Journal of Geophysical Research: Oceans, 115(C11): C11011, doi: 10.1029/2009JC006074
Nicolaus M, Petrich C, Hudson S R, et al. 2013. Variability of light transmission through Arctic land-fast sea ice during spring. The Cryosphere, 7(3): 977–986, doi: 10.5194/tc-7-977-2013
Nürnberg D, Wollenburg I, Dethleff D, et al. 1994. Sediments in Arctic sea ice: Implications for entrainment, transport and release. Marine Geology, 119(3–4): 185–214, doi: 10.1016/0025-3227(94)90181-3
Osterkamp T E, Gosink J P. 1984. Observations and analyses of sediment-laden sea ice. In: Barnes P W, Schell D M, Reimnitz E, eds. The Alaskan Beaufort Sea: Ecosystems and Environments. Pittsburgh, PA, USA: Academic Press, 73–93
Perovich D K. 1990. Theoretical estimates of light reflection and transmission by spatially complex and temporally varying sea ice covers. Journal of Geophysical Research: Oceans, 95(C6): 9557–9567, doi: 10.1029/JC095iC06p09557
Perovich D K. 1991. Seasonal changes in sea ice optical properties during fall freeze-up. Cold Regions Science and Technology, 19(3): 261–273, doi: 10.1016/0165-232X(91)90041-E
Perovich D K, Gow A J. 1996. A quantitative description of sea ice inclusions. Journal of Geophysical Research: Oceans, 101(C8): 18327–18343, doi: 10.1029/96JC01688
Perovich D K, Polashenski C. 2012. Albedo evolution of seasonal Arctic sea ice. Geophysical Research Letters, 39(8): L08501, doi: 10.1029/2012gl051432
Perovich D K, Richter-Menge J A. 2015. Regional variability in sea ice melt in a changing Arctic. Philosophical Transactions of the Royal Society A: Mathematical, Physical and Engineering Sciences, 373(2045): 20140165, doi: 10.1098/rsta.2014.0165
Perovich D K, Roesler C S, Pegau W S. 1998. Variability in Arctic sea ice optical properties. Journal of Geophysical Research: Oceans, 103(C1): 1193–1208, doi: 10.1029/97jc01614
Persson P O G, Fairall C W, Andreas E L, et al. 2002. Measurements near the atmospheric surface flux group tower at SHEBA: near-surface conditions and surface energy budget. Journal of Geophysical Research: Oceans, 107(C10): 8045, doi: 10.1029/2000JC000705
Qu Ping, Zhao Jinping, Li Shujiang, et al. 2009. Spectral features of solar radiation in sea ice of Bohai Sea. Haiyang Xuebao (in Chinese), 31(1): 37–43

Reimnitz E, McCormick M, McDougall K, et al. 1993. Sediment export by ice rafting from a coastal polynya, Arctic Alaska, U.S.A. Arctic and Alpine Research, 25(2): 83–98, doi: 10.2307/1551544

Rigor I G, Wallace J M. 2004. Variations in the age of Arctic sea-ice and summer sea-ice extent. Geophysical Research Letters, 31(9): L09401, doi: 10.1029/2004GL019492

Rothrock D A, Percival D B, Wensnahan M. 2008. The decline in Arctic sea-ice thickness: separating the spatial, annual, and interannual variability in a quarter century of submarine data. Journal of Geophysical Research: Oceans, 113(C5): C05003, doi: 10.1029/2007JC004252

Serreze M C, Holland M M, Stroeve J. 2007. Perspectives on the Arctic's shrinking sea-ice cover. Science, 315(5818): 1533–1536, doi: 10.1126/science.1139426

Stierle A P, Eicken H. 2002. Sediment inclusions in alaskan coastal sea ice: spatial distribution, interannual variability, and entrainment requirements. Arctic, Antarctic, and Alpine Research, 34(4): 465–476, doi: 10.1080/15230430.2002.12003518

Stroeve J, Holland M M, Meier W, et al. 2007. Arctic sea ice decline: faster than forecast. Geophysical Research Letters, 34(9): L09501, doi: 10.1029/2007GL029703

Stroeve J, Notz D. 2018. Changing state of Arctic sea ice across all seasons. Environmental Research Letters, 13(10): 103001, doi: 10.1088/1748-9326/aade56

Xu Zhantang, Yang Yuezhong, Wang Guifen, et al. 2012. Optical properties of sea ice in Liaodong Bay, China. Journal of Geophysical Research: Oceans, 117(C3): C03007, doi: 10.1029/2010jc006756

Zhao Jinping, Li Tao. 2010. Solar radiation penetrating through sea ice under very low solar altitude. Journal of Ocean University of China, 9(2): 116–122, doi: 10.1007/s11802-010-0116-7